ACS Sustainable Resource Management

pubs.acs.org/acssrm

Article

Incorporation of Cellulose Nanocrystals into a Cottonseed Oil-Based Network Polymer: Effect on Mechanical Properties

Katherine S. Elmore, Shuaib A. Mubarak, Gregory Schueneman, Yunsang Kim, and Santanu Kundu*

Cite This: *ACS Sustainable Resour. Manage.* 2024, 1, 1121−1130

Read Online

ACCESS | Metrics & More | Article Recommendations | Supporting Information

ABSTRACT: The detrimental issues surrounding the accumulation of traditional plastic waste are well known. A myriad of research has been conducted in the past few decades related to the synthesis of polymers using plant oils as starting monomers to obtain polymers from renewable sources. These polymers can be biodegradable and, therefore, can decrease further plastic waste accumulation. Although many studies have been conducted on the polymerization of soybean oil (SBO), comparatively few studies have been conducted on the polymerization of cottonseed oil (CSO). CSO is an excellent candidate for a plant-based polymer due to the abundance, renewability, and potential biodegradability of the synthesized polymers. We have synthesized cottonseed oil network polymer (CNP) from epoxidized cottonseed oil (ECSO) using maleic anhydride (MAL) as a crosslinker. Further, cellulose nanocrystals (CNCs) have been successfully incorporated into CNPs to produce a nanocomposite. Neither solvent exchange of the aqueous CNCs nor surface compatibilization was required before mixing with the ECSO and subsequently with maleic anhydride (MAL). FTIR confirmed the presence of CNCs in the polymer matrix, and the effects of CNCs on the mechanical properties were investigated. CNCs alter the mechanical properties of the crosslinked polymer, with an increase in stiffness/modulus correlating with an increasing CNC content. The polymer's thermal properties, as investigated by thermodynamic analysis and differential scanning calorimetry, have not undergone significant changes for the CNC concentrations considered here. Overall, this study demonstrates that CNC can be successfully incorporated into a network polymer derived from CSO, resulting in altered mechanical properties and demonstrating the possibility of tailoring them for various applications.

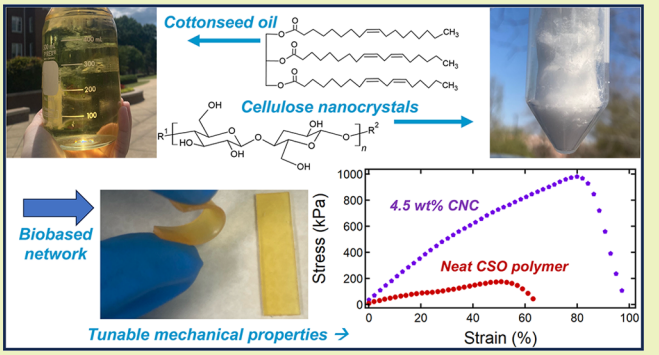

KEYWORDS: *cottonseed oil, plant oil epoxidation, crosslinked polymer, cellulose nanocrystals, mechanical properties*

INTRODUCTION

The environmental challenges associated with traditional plastics are well known. Since mass production began around the 1950s, over 8.3 billion metric tons of plastic have been produced.[1,2] Of this, approximately 65% have either been incinerated, releasing large volumes of greenhouse gas emissions,[1] or left untreated, which, in addition to releasing emissions,[3] builds up in landfills, the ocean,[4] or soil.[5] This has caused environmental casualties with a scope and severity that only grows as more single-use, non-biodegradable plastic is produced each year. Efforts to combat these issues over the past few decades have led to many polymers from renewable sources.[6−9] Polymers from greener feedstocks have been designed to degrade more readily and with lower hazardous byproducts, reducing environmental footprints.[10−13]

Plant oils are ideal candidates as a starting material for polymers because of their chemical functionality, abundance, renewability, and the resulting products potentially to be biodegradable and recyclable. Regarding the selection of plant oil, soybean oil (SBO) has been used in many polymer syntheses,[14−21] and is even used in some on-market products such as paint.[22] However, the problem with SBO as a starting material is that it is a significant contributor in the food industry (directly and as a textural or emulsification additive)[23] as well as the biofuel industry (where biodiesel is produced via transesterification reaction with SBO).[24] Particularly, in the year 2022, approximately 54% of SBO sourced in the United States was used for food, feed, and industrial uses, while 37% was used for biofuel.[25] In comparison, cottonseed oil (CSO), although it has not been investigated to the same extent as SBO,[26−29] has a similar chemical composition. However, it is both produced and consumed in much smaller quantities, indicating an opportunity for market expansion in this area.

Received: February 5, 2024
Revised: May 3, 2024
Accepted: May 6, 2024
Published: May 16, 2024

Additionally, while SBO is an integral part of the food industry as an additive in many products, CSO is not used for this purpose. Therefore, if CSO were to be used on a large scale in the synthesis of polymers, then this would not cause a disruption to the food supply chain. Specifically, 5.01 million metric tons (MMT) of CSO was produced in 2022 compared to 61.49 MMT of SBO.[30] As CSO-based materials will not compete with food sources, there is a significant opportunity for the growth of those materials.

The CSO is susceptible to chemical reactions because of the carbon−carbon double bonds (unsaturation) located on its triglyceride fatty acid chains. Specifically, CSO contains over 50% linoleic acid (two locations of unsaturation), approximately 20% each palmitic acid (no double bonds) and oleic acid (one double bond), as well as smaller amounts of stearic (no double bond), and linolenic acids (3 locations of unsaturation).[29] Epoxidation of CSO (or other plant oils) is a common preparation method that transforms the carbon−carbon double bonds into oxirane epoxy groups, greatly improving the monomers' crosslinking ability. Subsequently, various methods of crosslinking reactions have been utilized, leading to a wide range of products, such as UV curable materials,[31] resins,[32−34] coatings,[35,36] functional rubbers,[37] and composite matrices.[38]

Although an excellent option with respect to degradability, an argument against plant oil polymers is that their mechanical performance may not always be favorably compared to those of traditional plastics.[39−41] Nanomaterials have been demonstrated to significantly modify a polymer's physical properties, and cellulose nanocrystals (CNCs) have specifically been used in numerous plant oil polymerization studies,[42] e.g., in reactions with ESBO-based resins,[43] polyurethanes,[44] and (meth)acrylate polymers,[45] UV-cured acrylated ESBO thermosets,[46] sunflower-derived epoxy polymers,[47] castor oil-based polyurethanes,[48−50] and resins from tung-oil.[51] Because of CNCs' excellent tensile strength (greater than that of Kevlar[52]), significant improvements in mechanical properties have been observed with the incorporation of CNCs. For example, tensile moduli have shown improvements anywhere from 5% on the lower end,[40] to more extreme changes. One study resulted in an increase from 0.34 to 630 MPa after CNCs had been incorporated.[51]

However, CNCs can be difficult to incorporate into polymers because of their hydrophilic nature. To address this issue, processes have been developed to successfully improve the interactions between the CNCs and the reacting media and polymer. These include surface modification/compatibilization, which improves the dispersion of CNCs within the reaction medium, thus preventing major CNC agglomeration,[48,53−57] as well as methods to facilitate the formation of covalent bonds between the polymer matrix and CNCs (e.g., grafting polymers onto CNCs or using crosslinkers).[57] Covalent bonding between CNCs and polymers such as natural rubber and PLA has been shown to improve mechanical properties (e.g., modulus, tensile strength, and elongation at break) beyond what physical interactions alone would achieve.[58,59] In addition to improving or altering the mechanical properties of polymers, it has been demonstrated that CNCs also improve the biodegradability of the polymers into which they are incorporated.[60−62] Although there are reports on CNCs incorporated during polymerizations of some other plant oils, such as with SBO (epoxidized and mixed with polylactide,[40] high oleic,[63] acrylated,[64] and modified via thiol−ene click chemistry[45]), foamed polyurethanes from castor oil,[50] or sunflower oil,[65] a CNC-incorporated cotton oil-based polymers with evidence of good CNCs dispersity has not been reported widely in the literature.

In an earlier study, CSO network polymer was synthesized by first epoxidizing the CSO, followed by crosslinking with maleic anhydride (MAL) in varying molar ratios.[66] Polymers with ultimate tensile strengths (UTS) of up to 0.4 MPa, stretch ratios of up to 125%, and elastic moduli on the order of 1 MPa were obtained. Here, we report the synthetic route to incorporate CNCs in CSO network polymer. No additional steps, such as solvent exchange or functionalization of the CNCs' surface groups, were required before incorporating the post-dialyzed freeze-dried CNCs with the ECSO and MAL. An investigation of the corresponding change in mechanical and thermal properties was conducted. Particularly, the mechanical and thermal properties for a range of CNCs concentrations are presented.

EXPERIMENTAL SECTION

Materials. CSO (Acros Organics), glacial acetic acid, sulfuric acid (BDH brand), and 50 wt % aqueous hydrogen peroxide solution were purchased from Fisher Scientific. An aqueous solution of 10 wt % sulfuric-acid hydrolyzed CNCs (1.06 wt % sulfur on dry CNCs, sodium form) was received from Forest Product Laboratories (2018-FPL-CNC-130 from CNC-115D). Maleic anhydride (MAL) was purchased from Fisher Scientific (Alfa Aesar).

Preparation of Freeze-Dried CNCs. Sulfuric-acid hydrolyzed CNCs were diluted from 10 wt % to 1 wt % by vortex mixing with deionized water. Dialysis was performed to remove free sulfate groups from the CNCs.[67] This was done by placing the dilute 1 wt % concentration of aqueous CNCs into Biotech 100 kDa cellulose ester (CE) dialysis membrane tubing, followed by placing the tubing into a container of deionized water. The water in the container was refreshed daily for 1 week. Conductometric titration was performed before and after dialysis using a conductometer (Oakton PC2700) to determine the reduction of sulfur content (see Figure S1 of the Supporting Information, SI). After dialysis, the deionized CNCs were further diluted to 0.5 wt %. This aqueous solution was then freeze-dried using a Labconco FreeZone Plus 4.5 L drier at −40 °C and 0.018 mbar for 3 days to dry the CNCs completely.

Preparation of ECSO. A predetermined mass of CSO was added to a three-necked round-bottom flask over a hot plate. Using a magnetic stirrer, CSO was stirred at ∼300 rpm. To this, glacial acetic acid was added to the flask and a molar ratio of 1:2 for CH3COOH (acetic acid) to C═C in CSO was maintained. Sulfuric acid was added next to achieve 2 wt % concentration, as calculated from the total mass of the reaction mixture. The reaction was heated to 55 °C, and then aqueous hydrogen peroxide (concentration of 50 vol %) at a mole ratio of 1.5:1 for H_2O_2:C═C was added dropwise over approximately 20 min. The mixture was left to react overnight. After the reaction was complete, water washing and solvent extraction with ethyl acetate was used to respectively remove acids and water. This was followed by rotary evaporation to remove the solvent.

Preparation of CNC-Incorporated CNP. The freeze-dried CNCs was added to the epoxidized CSO (ECSO) in small mg increments to avoid agglomeration. The solution was probe sonicated intermittently between adding CNCs using a Fisherbrand FB505 Sonic Dismembrator, 500 Watts, 20 kHz, at 60% amplitude for a 5 s pulse duration. One pulse per addition of CNCs with an additional 3−5 pulses following the last CNCs' addition was used. It is important not to vortex mix before probe sonication and to add the CNCs in small stepwise increments to achieve minimum CNC agglomeration/optimum CNC dispersion (according to visual observations, vortex mixing before probe sonication appeared to inhibit dispersion of CNCs and increase agglomeration). Rheometric analysis was conducted at room temperature using a TA-Instruments DHR2 and

https://doi.org/10.1021/acssusresmgt.4c00047
ACS Sustainable Resour. Manage. 2024, 1, 1121−1130

Scheme 1. Reaction for the Synthesis of CNC-Incorporated CSO Network Polymers

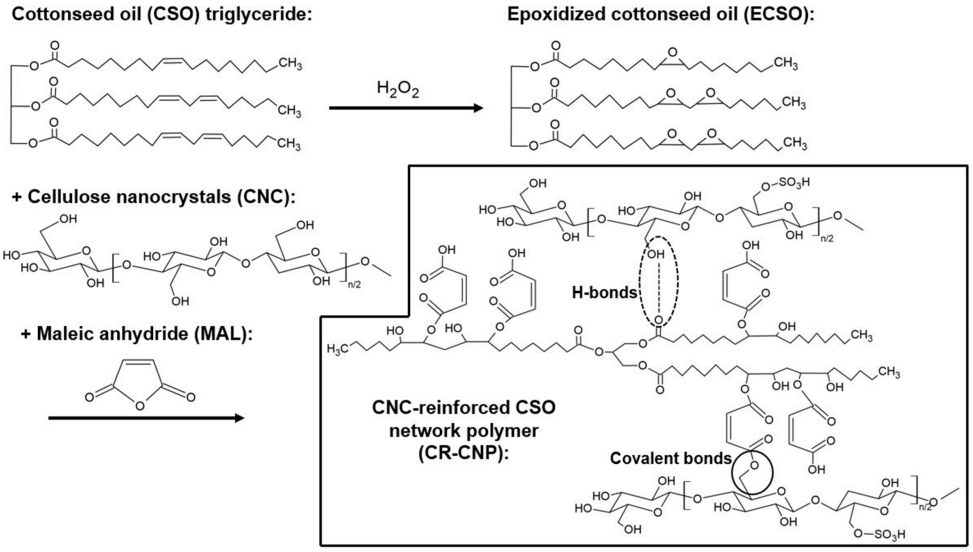

parallel plate geometry to observe the changes in ECSO viscosity after the addition of CNCs. Samples were analyzed under a shear rate from 1 to 100 s^{-1} at 30 °C. Although not by a significant amount, there was a slight increase in viscosity observed with the addition of CNCs (see SI Figure S2).

Next, MAL was added in a previously determined optimum ratio of 2:5 by mol (ECSO:MAL).[66] This is followed by heat mixing in a silicone oil bath on a hot plate at 80 °C and ∼300 rpm for 1.5 h. Then, the mixture was poured onto a flat metal plate lined with aluminum foil (folded up on the sides to prevent spreading beyond the intended geometry) and placed under a 25 inHg vacuum overnight to remove any air bubbles. Finally, the polymer was cured at 150 °C for 18 h. The polymer samples for varying CNC concentrations are referred to by their concentrations (e.g., 0.1 wt % refers to the 0.1 wt % CNCs in ECSO polymer samples).

Characterizations. Fourier transform infrared spectroscopy (FTIR) was carried out with a Nicolet iS 5 spectrometer, with spectra collected from 400−4000 cm^{-1}. The microstructure of the CNC-containing polymer was observed using TEM. CNC-containing polymer samples were stained using uranyl acetate to enhance the contrast between CNCs and surrounding polymer. The samples were then embedded into LR-White resin. From this, 100 nm thick sections were microtomed using a Reichert Jung Ultracut-E ultramicrotome equipped with a diamond blade and then placed on a copper grid. Both samples were analyzed using a JEOL 2100 TEM, operated at 200 kV accelerating voltage.

For atomic force microscopy (AFM) measurements, one droplet of diluted CNC (c.a. 0.02%) was spin-coated onto a silicon wafer, which had been freshly treated with a piranha solution and then dipped in an aqueous polyethylenimine solution (1%).[68] The spun CNC film was baked at 120 °C for 20 min. AFM measurements were performed using a Bruker Dimension Icon (Hamburg, Germany) in a tapping mode.

A Mark-10 tensile instrument (Model DC4050, 2.5 kN cell load) was used to conduct the tensile testing of the samples. Post-cured polymer specimens with a thickness of 1.3 +/− 0.2 mm were cut into 25.4 mm length × 6.4 mm wide (1 inch × 1/4 inch) rectangular geometries. The tensile tests were conducted at a rate of 10 mm/s.

The thermal behavior of the samples was analyzed using thermal gravimetric analysis (TGA) and differential scanning calorimetry (DSC) on TA Instruments' Q600 SDT and Q2000 models, respectively. Both thermal analyses were conducted under an inert atmosphere of continuously flowing (50 mL/min) ultra-high purity nitrogen gas. For TGA experiments, the samples (4−9 mg) were heated from room temperature (approximately 25 °C) to 600 °C at a rate of 10−20°C/min. For DSC analysis, the neat and CNC-incorporated polymer samples (∼5−10 mg) were hermetically sealed in aluminum pans. The samples were equilibrated at 40 °C for 5 min and then heated to 150 °C at a rate of 20 °C/min. The samples were held at this temperature for another 5 min, then cooled at the same rate to -50 °C, and then again held isothermal for 5 min before heating again. This cycle was repeated three times for all samples.

RESULTS AND DISCUSSION

Incorporation of CNCs at Varying Concentration in CNP. The proposed reaction mechanism for the incorporation of CNCs in CSO network polymer (CNP) is shown in Scheme 1. Plant oils are composed of triglycerides that contain long aliphatic fatty acid (FA) chains connected via ester linkages to a glycerol backbone. Located on these FAs are unsaturated carbon−carbon double bonds, which may be utilized for polymerization reactions. Since the main types of FAs found in CSO are linoleic, followed by oleic acid (two and one carbon−carbon double bond, respectively, on an 18-carbon chain), the presumed structure of a CSO triglyceride is one oleic and two linoleic FA per CSO monomer.[69] The CSO used in this study was determined to have an iodine value between 109−120, and a density of 0.92 g/cm^3.[66] The CSO triglyceride was first prepared for polymerization via an epoxidation reaction to synthesize the network polymer. The monomer was reacted with hydrogen peroxide, which acts as an oxygen donator to convert the carbon−carbon double bonds to oxirane rings. These rings are significantly more reactive than the carbon−carbon double bonds.[70] This epoxidized CSO monomer (ECSO) contains five oxirane groups per triglyceride monomer and, thus, five potential locations where a crosslinking reaction may occur.

MAL was selected as a bifunctional crosslinker between the ECSO triglyceride molecules and the CNCs, enabling the formation of a crosslinked network polymer. MAL is a good candidate for crosslinker because of its low toxicity and its wide commercial availability.[71,72] The specific reaction between the MAL and the ECSO oxirane groups is nucleophilic substitution and has been utilized earlier to obtain CNPs.[66] Here, we expect the covalent bond formation between the MAL and CNCs through ring-opening esterification,[59] wherein the CNCs hydroxyl groups react with the MAL anhydride groups (Scheme 1).[72] Further, CNCs can also form hydrogen

https://doi.org/10.1021/acssusresmgt.4c00047
ACS Sustainable Resour. Manage. 2024, 1, 1121−1130

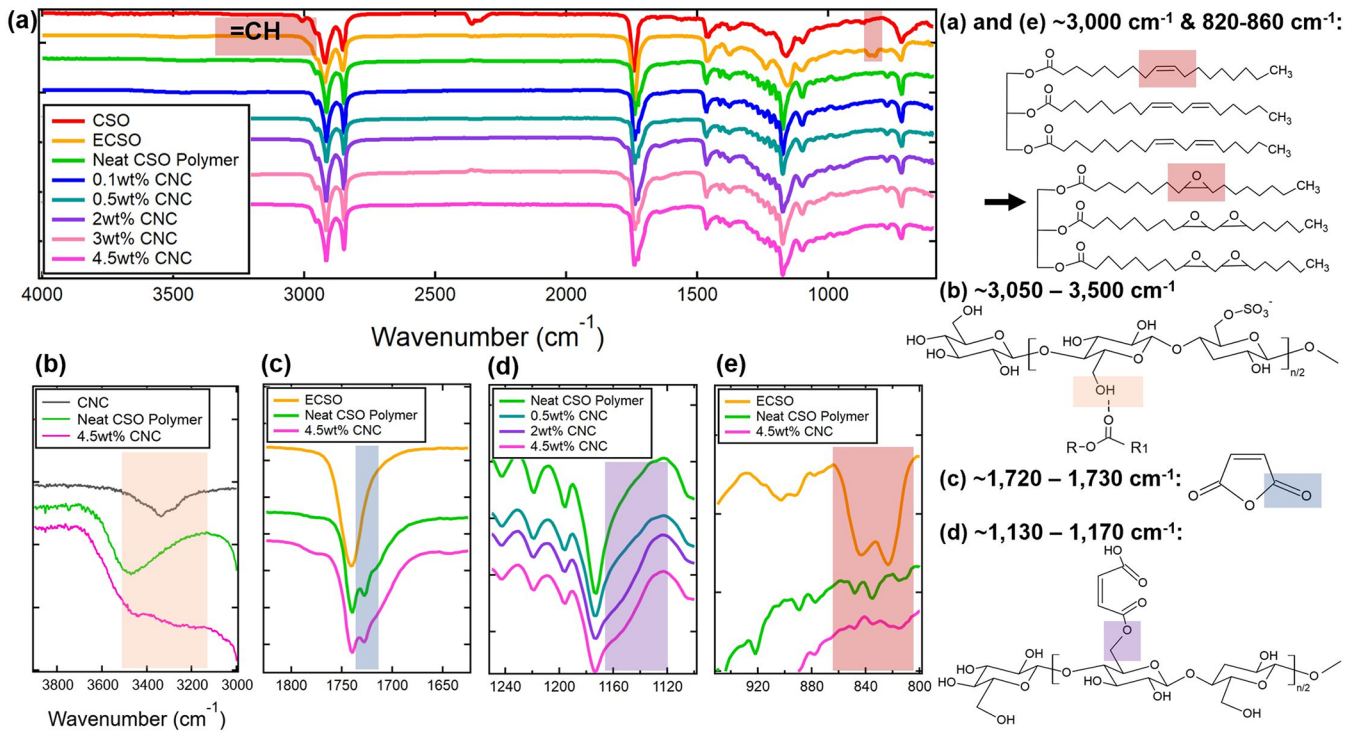

Figure 1. FTIR data for ECSO, crosslinked polymers without and with various concentrations of CNCs. Full spectra and zoomed views of the functional group peaks are shown on the left side of the figure, while on the right side are corresponding schematics showing the chemical structures. The specific functional groups are shaded: (a) & (e) (red shading) C═C bond at 3000 cm^{-1} and epoxies (or oxirane rings) between 820−850 cm^{-1}; (b) (orange shading) −OH stretching likely due to of ring-opened oxirane (chemical structure not shown) and H-bonded CNCs at the range of 3050−3,500 cm^{-1}; (c) (blue shading) C═O bond of ester between 1700−800 cm^{-1}; and (d) (purple shading) C−O−C of ether at 1120−1200 cm^{-1}. Results for ECSO are also shown for comparison purposes.

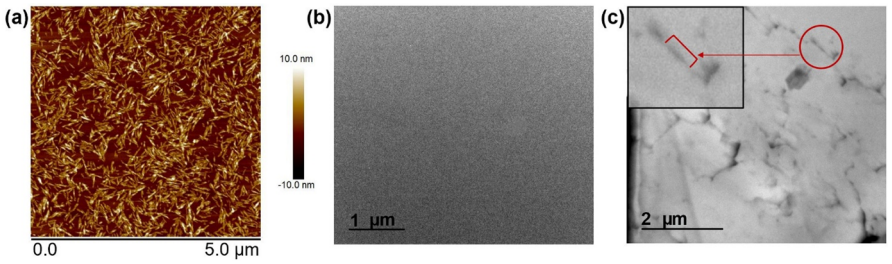

Figure 2. (a) Typical AFM image of CNCs, (b) TEM image of neat polymer (0 wt % CNCs), and (c) 4.5 wt % polymer. A zoomed image of CNCs is shown in the inset of (c). The darker regions in the TEM image capture CNCs.

bonds with the carbonyl groups in the surrounding polymer network due to the large number of hydroxyl groups present on the surface of the nanocellulose structure (Scheme 1).[73] Similar hydrogen bond formation has been reported by Cao[59] and Khan.[73]

FTIR analysis was performed on the CSO, ECSO, crosslinked polymers with and without varying concentrations of CNCs, and other components, and results are shown in Figure 1. As observed in Figure 1a, after epoxidation but preceding polymerization, the CSO's ═CH peak at 3000 cm^{-1} disappears, while two peaks representing epoxy functionalities appear at 820−860 cm^{-1}.[59,74] After the polymerization reaction, the epoxy peaks at 820−860 cm^{-1} significantly decrease in intensity (Figure 1e). Additionally, after polymerization, a peak at 1730 cm^{-1} develops, representing the C═O bond stretch of the ester functional group (Figure 1c). For CNCs, a broad peak from 3100 -3450 cm^{-1} was observed, whereas for the polymer without CNCs, a peak from 3050 to 3650 cm^{-1} was noted. However, for 4.5% CNC-containing polymer, no distinct peak was observed in that region, but an increase of intensity over the range of 3050−3500 cm^{-1} was noticed, likely capturing a broad peak. The peak in this region has been associated with −OH group stretching, and the literature reports indicate that the peak can shift to a lower wavenumber because of hydrogen bonding.[75−77] The broad-band observed here suggests the presence of H-bonded structures and ring-opened oxirane structures in the sample. Also, for CNC-incorporated samples, a shoulder peak appears around 1150 cm^{-1} in the region representing the C−O bond of ester groups (Figure 1d). This peak appears only when the CNCs are present within the polymer sample and generally increases in intensity with increased CNC concentration. Individual figures for each spectrum are presented in Supporting Information (SI) Figure S3.

The decrease of the C═C peak at 3000 cm^{-1} and the formation of epoxy peaks at 820−860 cm^{-1} after epoxidation

https://doi.org/10.1021/acssusresmgt.4c00047
ACS Sustainable Resour. Manage. 2024, 1, 1121−1130

indicate the conversion of the carbon−carbon double bond groups into oxirane,[32,40,85,86,66,78−84] thus confirming the success of the epoxidation reaction. After polymerization, there is a decrease in intensity of the epoxy peaks at 820−860 cm^{-1}. This decrease in epoxy peaks after polymerization indicates that ring opening of the oxirane groups occurs during the polymerization reaction, but as the peak has not completely disappeared, some oxirane rings may still be present in the system. Post-polymerization, the new peak formed at 1730 cm^{-1} appears due to the addition of MAL, as the carboxylic groups within MAL's structure are in a distinct chemical environment compared to the carboxyl groups found on the CSO triglyceride.[66,87] Finally, the shoulder peak appearing at 1150 cm^{-1} after polymerization and only with the CNC-containing polymer samples (Figure 1e) further confirms the presence of CNCs in the polymer. The CNCs' C−O ester groups are in a different environment compared to the neat CSO polymer C−O groups because of covalent bond formation. The intensity of this shoulder peak increases with increasing CNC concentration, indicating more occurrence of covalent bond formation.[88]

Structural Characterization. Figure 2a shows a typical atomic force microscopy (AFM) image of CNCs. A TEM image of 4.5 wt % polymer is shown in Figure 2c. Here, the CNCs are found to be dispersed throughout the specimen, with individual CNC particles appearing to be identifiable, indicating no significant agglomeration. Similar TEM images revealing distinguishable CNCs dispersed throughout a polymer sample have been reported in literature for poly(ε-caprolactone),[89] rubber latex,[90] and a polyester synthesized from polyols and sebacic acid[91] to name a few examples. Additionally, in some instances, there appears to be end-to-end contact between and localized alignment among CNC particles, which may suggest the percolation in the sample.[89,90,92] The aspect ratios for CNC specimens typically range between 5 to 70, depending on the source.[52,53,67,93] Beyond the percolation threshold (V_c), CNCs can also form a three-dimensional (3D) network. For a cylindrical geometry, $V_c = 0.7/A$,[94] where A is the CNCs' aspect ratio (see SI). For our case, the aspect ratio for the CNCs was estimated to be ∼20, which leads to a percolation threshold of approximately 5 wt % (SI).[93,95,96] The aspect ratio for the polymers was estimated by using a composite average of identifiable individual CNCs particles observed in Figure 2c as well as additional TEM images taken of the 4.5 wt % polymer in several locations along the sample. Additional analysis to capture the morphological differences between the neat and CNC-incorporated polymers was performed using scanning electron microscopy (SEM). The surface of the CNCs-containing polymer is notably rougher than the neat polymer (SI Figure S4). This indicates the successful inclusion of CNCs, leading to their presence near the surface.

Mechanical Properties. Tensile testing was conducted for polymers with each concentration of CNCs as well as the polymers without CNCs, and the results are shown in Figure 3. Properties, including Young's Modulus (YM), ultimate tensile strength (UTS), strain, and toughness, were determined at varied concentrations of CNCs and are shown in Figure 4. Although the YM for 0.1 and 0.5 wt % appear similar in Figure 4a, *t*-test analysis indicated statistically significant differences for all their mechanical properties (see SI Table S1). Overall, with increasing CNCs content, both YM and UTS increased. The toughness also appears to increase as the CNC concentration increases, while the extensibility either increases slightly or is not significantly affected as more CNCs are added. At the highest concentration tested of 4.5 wt %, the average values observed were YM ∼1.81 ±. 0.204 MPa, UTS ∼1.09 ± 0.185 MPa, toughness ∼583 ± 66.1 kPa, and strain at break ∼94 ± 5%.

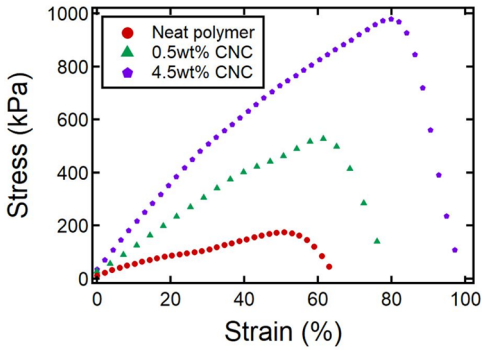

Figure 3. Typical tensile stress vs. strain curves (smoothed data) of CNP and CNC-incorporated CNP for varying CNC concentrations.

The increase in YM and UTS with increasing CNC concentration is expected given CNCs' significant tensile strength (as theoretically modeled or empirically measured by Raman spectroscopy) and stiffness (as empirically measured using multiple methods).[52,97] Usually, an increased number of crosslinks leads to higher modulus but a decrease in stretchability. In our case, a similar or slight increase in extensibility can be associated with the physical bonding of CNCs, which dissociate and reform, dissipating energy and improving extensibility.[59,73,96,98] Thereby, these composites exhibit a rare escape from the trade-off between improved modulus and sacrificed ductility or toughness. An overall trend of increase in mechanical properties with an increase in CNC content to 4.5 wt % was observed; however, a slight decrease for 0.5 wt % CNC content has been noted. This behavior is consistent with the trends observed in the literature, where the change in mechanical properties was reported to be non-monotonic with increasing CNC content.[99−102] This has been attributed to the reaching percolation threshold and agglomeration of CNCs beyond that.[44,60] However, the estimated threshold calculated for the CNCs in this study is higher than 0.5 wt %; therefore, the exact reason behind the drop in modulus at 0.5 wt % CNC content will require further investigation in the future.

Thermal Properties. The thermal stability of the CNCs, neat polymer, and 4.5 wt % polymer was determined using TGA. As shown in Figure 5a, the degradation of CNCs occurs in three phases: immediately and up to around 200 °C, 200−300 °C, and then from 300 °C continuing past the temperature range shown here. For both the neat and 4.5 wt % polymers, the decomposition began at approximately 150 °C, with approximately 10 and 15 wt % reduction occurring for the neat and 4.5 wt % polymers by 300 °C, respectively. From there, the 4.5 wt % polymer degrades at a slightly faster rate compared to the neat polymer, resulting in a slightly higher final residual mass at ∼485 °C.

The thermal degradation behavior of the CNCs (Figure 5a) is typical to that reported previously, with an initial mass loss for the sample up to ∼200 °C attributed to moisture evaporation,[103] followed by decomposition of the CNCs' glucose units within the cellulose backbone, initiated by free

https://doi.org/10.1021/acssusresmgt.4c00047
ACS Sustainable Resour. Manage. 2024, 1, 1121−1130

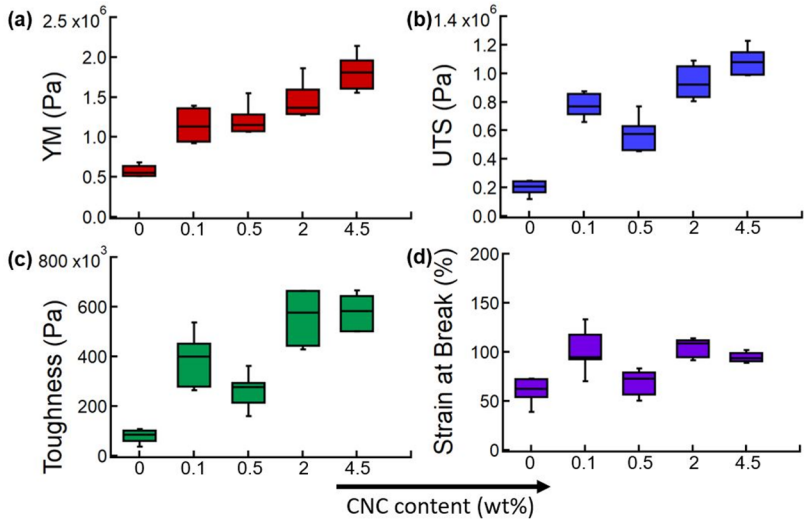

Figure 4. Statistical summary of values obtained for (a) Young's modulus (YM), (b) ultimate tensile strength (UTS), (c) toughness, and (d) strain at break for CNC-incorporated CNPs. The average values are shown, and the error bars represent the standard deviation. At least seven specimens were tested for each concentration of CNCs.

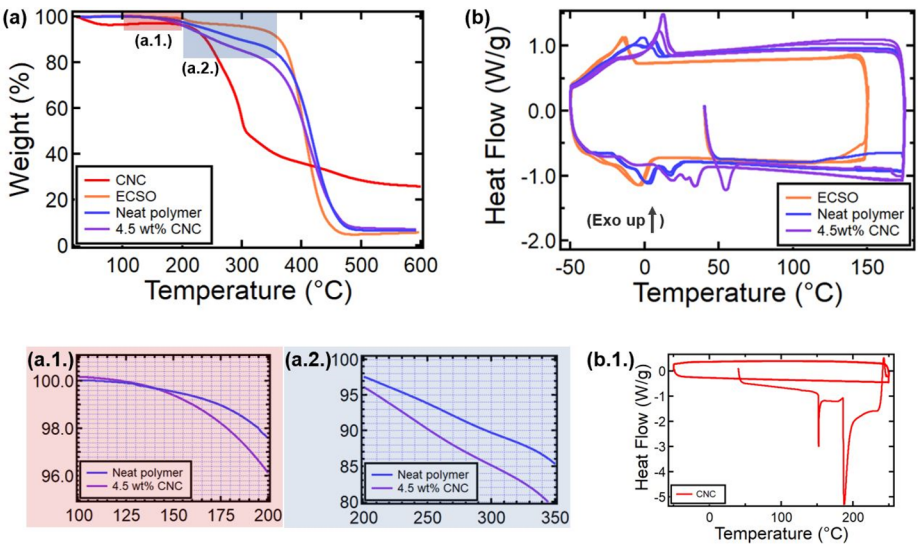

Figure 5. (a) Representative TGA and (b) DSC of neat and CNC-incorporated CNPs in varying concentrations. (a.1 and a.2) Zoomed in view of selected temperature ranges. b.1. is the DSC thermograph of neat CNCs. Results for ECSO are also shown for comparison purposes. The DSC results are shown for three cycles.

chain ends on the CNCs' surface.[104−107] Higher residual CNCs' mass is due to remaining surface sulfate groups.[108] Comparing the neat and 4.5 wt % polymers, the greater mass loss at lower temperatures for the 4.5 wt % is likely the result of the degradation of CNCs within the polymer matrix, as has been previously observed with the incorporation of chemically unmodified CNCs in maleic anhydride grafted poly(butylene adipate-*co*-terephthalate) (PBAT) or poly(ε-caprolactone) (PCL) matrices.[87,109] Although it appears that only a slight difference may be observed between the polymer containing CNCs and the neat polymer's residual mass, this corroborates with expected calculations (see SI Figure S5).

DSC was used to further characterize the thermal properties of the polymers (Figure 5b; see SI Figure S6 for individual DSC trace). For the neat polymer, a glass transition temperature (T_g) was observed at approximately −10 °C. The T_g of the 4.5 wt % polymer was slightly higher at −5 °C. Two melting peaks occur in the neat polymer sample at 5 °C and 15 °C. Both peaks are greater than the melting temperature (T_m) of the ECSO at approximately −5 °C. Recrystallization of the neat polymer (T_c) occurs in two stages at 10 °C and 0 °C. For the 4.5 wt % polymer, a single T_m was observed for the first heating cycle at 55 °C. However, multiple Tm at 15 °C, 25 °C, and 30°C were observed in the second heating cycle. Note that a slight variation in T_g and T_m has been observed between different batches of samples. The DSC results for the CNCs in Figure 5b.1 showed no significant transitions other than evaporation of bound water within the CNCs from approximately 145−190 °C.[110,111]

Comparing the DSC results for the neat polymer (Figure 5b), the increase in T_g and T_m for the 4.5 wt % polymer compared to the neat polymer can be attributed to the incorporation of CNCs, resulting in modified network structures.[109] The existence of melting and recrystallization peaks for both the neat and 4.5 wt % polymers indicate the presence of crystal-like, non-crosslinked FA chains both

https://doi.org/10.1021/acssusresmgt.4c00047
ACS Sustainable Resour. Manage. 2024, 1, 1121−1130

polymers since a truly crosslinked polymer with short chain lengths between the crosslink points will likely not have a melting temperature. Multiple melting and recrystallization peaks likely indicate the presence of imperfections within the network, as well as locally existing crystalline domains, as anticipated for these complex nanocomposite samples. For the 4.5 wt % polymer, the apparent disappearance of the melting peak at 55 °C from the first heating cycle to the second may be due to kinetically frozen FA chains during the crosslinking process.

CONCLUSIONS

In this study, a CNC-reinforced network polymer was successfully synthesized from ECSO. An overall increase in mechanical properties, including YM, UTS, and toughness, was observed with increasing CNC concentration. Strain at break either slightly improved or was not significantly affected by increased CNC content. The highest YM, UTS, and toughness were achieved with a CNC concentration of 4.5 wt %, while the greatest failure strain was observed at 2 wt % CNCs. Thermal stability of the polymers was maintained at even the highest CNC concentration tested. These results demonstrate that tunability and enhancement of the CSO network polymer's mechanical properties are achievable by using CNCs in varying concentrations.

ASSOCIATED CONTENT

Supporting Information

The Supporting Information is available free of charge at https://pubs.acs.org/doi/10.1021/acssusresmgt.4c00047.

Estimation of SO_4 content of CNCs before and after dialysis estimated via conductometric titration; viscosity as a function of shear rates for ECSO and 4.5 wt % CNCs in ECSO; individual FTIR spectra for each component of the nanocomposites compared to the resulting polymers at varying concentrations of CNCs; estimation of the percolation threshold; SEM images of the neat and CNC-incorporated polymers; statistical analysis comparing the mechanical properties of 0.1 and 0.5 wt % CNCs polymers; zoomed-in TGA data showing actual final mass and their comparison to the estimated final mass; and DSC data for each component of the nanocomposite and final polymers (PDF)

AUTHOR INFORMATION

Corresponding Author

Santanu Kundu − *Dave C. Swalm School of Chemical Engineering, Mississippi State University, Mississippi State, Mississippi 39762, United States;* orcid.org/0000-0002-0767-0512; Email: santanukundu@che.msstate.edu

Authors

Katherine S. Elmore − *Dave C. Swalm School of Chemical Engineering, Mississippi State University, Mississippi State, Mississippi 39762, United States*

Shuaib A. Mubarak − *Department of Sustainable Bioproducts, Mississippi State University, Starkville, Mississippi 39759, United States;* orcid.org/0000-0002-4068-158X

Gregory Schueneman − *Forest Products Laboratory, USDA United States Forest Service, Madison, Wisconsin 53726, United States;* orcid.org/0000-0002-6390-5240

Yunsang Kim − *Department of Sustainable Bioproducts, Mississippi State University, Starkville, Mississippi 39759, United States;* orcid.org/0000-0002-5330-1670

Complete contact information is available at: https://pubs.acs.org/10.1021/acssusresmgt.4c00047

Funding

The authors would like to gratefully acknowledge the partial funding for this work provided by IHL SMART.

Notes

The authors declare no competing financial interest.

ACKNOWLEDGMENTS

The authors would like to thank Dr. Rooban Venkatesh KG Thirumalai (Institute for Imaging and Analytical Technologies, Mississippi State University), who was instrumental in obtaining the TEM data for this study.

REFERENCES

(1) Geyer, R.; Jambeck, J. R.; Law, K. L. Production, Use, and Fate of All Plastics Ever Made. *Sci. Adv.* **2017**, *3* (7), 25−29.

(2) Global plastic production 1950-2020 | Statista https://www.statista.com/statistics/282732/global-production-of-plastics-since-1950/ (accessed Mar 16, 2022).

(3) Royer, S. J.; Ferrón, S.; Wilson, S. T.; Karl, D. M. Production of Methane and Ethylene from Plastic in the Environment. *PLoS One* **2018**, *13* (8), e0200574.

(4) Ford, H. V.; Jones, N. H.; Davies, A. J.; Godley, B. J.; Jambeck, J. R.; Napper, I. E.; Suckling, C. C.; Williams, G. J.; Woodall, L. C.; Koldewey, H. J. The Fundamental Links between Climate Change and Marine Plastic Pollution. *Sci. Total Environ.* **2022**, *806*, No. 150392.

(5) Ali, S. S.; Elsamahy, T.; Koutra, E.; Kornaros, M.; El-Sheekh, M.; Abdelkarim, E. A.; Zhu, D.; Sun, J. Degradation of Conventional Plastic Wastes in the Environment: A Review on Current Status of Knowledge and Future Perspectives of Disposal. *Sci. Total Environ.* **2021**, *771*, No. 144719.

(6) Montero de Espinosa, L.; Meier, M. A. R. Plant Oils: The Perfect Renewable Resource for Polymer Science?! *Eur. Polym. J.* **2011**, *47*, 837−852.

(7) Raza, S.; Zhang, J.; Ali, I.; Li, X.; Liu, C. Recent Trends in the Development of Biomass-Based Polymers from Renewable Resources and Their Environmental Applications. *J. Taiwan Inst. Chem. Eng.* **2020**, *115*, 293−303, DOI: 10.1016/j.jtice.2020.10.013.

(8) Silva, J. A. C.; Grilo, L. M.; Gandini, A.; Lacerda, T. M. The Prospering of Macromolecular Materials Based on Plant Oils within the Blooming Field of Polymers from Renewable Resources. *Polym.* **2021**, *13* (11), 1722.

(9) Mosiewicki, M. A.; Aranguren, M. I. A Short Review on Novel Biocomposites Based on Plant Oil Precursors. *Eur. Polym. J.* **2013**, *49* (6), 1243−1256.

(10) Correa, J. P.; Montalvo-Navarrete, J. M.; Hidalgo-Salazar, M. A. Carbon Footprint Considerations for Biocomposite Materials for Sustainable Products: A Review. *J. Cleaner Prod.* **2019**, *208*, 785−794, DOI: 10.1016/j.jclepro.2018.10.099.

(11) Rosenboom, J. G.; Langer, R.; Traverso, G. Bioplastics for a Circular Economy. *Nat. Rev. Mater.* **2022**, *7* (2), 117−137.

(12) RameshKumar, S.; Shaiju, P.; O'Connor, K. E.; P, R. B. Bio-Based and Biodegradable Polymers - State-of-the-Art, Challenges and Emerging Trends. *Curr. Opin. Green Sustainable Chem.* **2020**, *21*, 75−81, DOI: 10.1016/j.cogsc.2019.12.005.

(13) Pellis, A.; Malinconico, M.; Guarneri, A.; Gardossi, L. Renewable Polymers and Plastics: Performance beyond the Green. *New Biotechnol.* **2021**, *60*, 146−158, DOI: 10.1016/j.nbt.2020.10.003.

(14) Alhanish, A.; Abu Ghalia, M. Developments of Biobased Plasticizers for Compostable Polymers in the Green Packaging Applications: A Review. *Biotechnol. Prog.* **2021**, *37* (6), No. e3210.
(15) Quirino, R. L.; Monroe, K.; Fleischer, C. H.; Biswas, E.; Kessler, M. R. Thermosetting Polymers from Renewable Sources. *Polym. Int.* **2021**, *70* (2), 167−180.
(16) Uyama, H. Functional Polymers from Renewable Plant Oils. *Polym. J.* **2018**, *50* (11), 1003−1011.
(17) Islam, M. R.; Beg, M. D. H.; Jamari, S. S. Development of Vegetable-Oil-Based Polymers. *J. Appl. Polym. Sci.* **2014**, *131* (18), 9016−9028.
(18) Lligadas, G.; Ronda, J. C.; Galià, M.; Cádiz, V. Renewable Polymeric Materials from Vegetable Oils: A Perspective. *Mater. Today* **2013**, *16* (9), 337−343.
(19) Ronda, J. C.; Lligadas, G.; Galià, M.; Cádiz, V. Vegetable Oils as Platform Chemicals for Polymer Synthesis. *Eur. J. Lipid Sci. Technol.* **2011**, *113* (1), 46−58.
(20) Meier, M. A. R.; Metzger, J. O.; Schubert, U. S. Plant Oil Renewable Resources as Green Alternatives in Polymer Science. *Chem. Soc. Rev.* **2007**, *36* (11), 1788−1802.
(21) Swain, S. N.; Biswal, S. M.; Nanda, P. K.; Nayak, P. L. Biodegradable Soy-Based Plastics: Opportunities and Challenges. *J. Polym. Environ.* **2004**, *12* (1), 35−42.
(22) Use Soy: Common Use Coatings https://soynewuses.org/common-uses/coatings/ (accessed Apr 1, 2023).
(23) Moyer, K. Soybean oil is the most widely used edible oil in the U.S. https://blog.aghires.com/soybean-oil-widely-used-edible-oil-u-s/.
(24) Hay, F. J. Soybeans for Biodiesel Production https://farm-energy.extension.org/soybeans-for-biodiesel-production/.
(25) U.S. Department of Agriculture Economic Research Service. Oil Crops Yearbook https://www.ers.usda.gov/data-products/oil-crops-yearbook/.
(26) Ebrahimnezhad-Khaljiri, H.; Ghadi, A. Recent Advancement in Synthesizing Bio-Epoxy Nanocomposites Using Lignin, Plant Oils, Saccharides, Polyphenols, and Natural Rubbers: A Review. *Int. J. Biol. Macromol.* **2024**, *256*, No. 128041.
(27) Ronda, J. C.; Lligadas, G.; Galià, M.; Cádiz, V. Vegetable Oils as Platform Chemicals for Polymer Synthesis. *Eur. J. Lipid Sci. Technol.* **2011**, *113* (1), 46−58.
(28) Xia, Y.; Quirino, R. L.; Larock, R. C. Bio-Based Thermosetting Polymers from Vegetable Oils. *J. Renew. Mater.* **2013**, *1* (1), 3−27.
(29) Xia, Y.; Larock, R. C. Vegetable Oil-Based Polymeric Materials: Synthesis, Properties, and Applications. *Green Chem.* **2010**, *12* (11), 1893−1909.
(30) Statista. Production of major vegetable oils worldwide from 2012/13 to 2022/2023, by type (in million metric tons) https://www.statista.com/statistics/263933/production-of-vegetable-oils-worldwide-since-2000/.
(31) Vonsul, M. I.; Webster, D. C. Investigation of Cottonseed Oil as Renewable Source for the Development of Highly Functional UV-Curable Materials. *Prog. Org. Coatings* **2023**, *185*, No. 107883.
(32) Pawar, M.; Kadam, A.; Yemul, O.; Thamke, V.; Kodam, K. Biodegradable Bioepoxy Resins Based on Epoxidized Natural Oil (Cottonseed & Algae) Cured with Citric and Tartaric Acids through Solution Polymerization: A Renewable Approach. *Ind. Crops Prod.* **2016**, *89*, 434−447.
(33) Mohamed, A. A.; Hussain, S.; Alamri, M. S.; Ibraheem, M. A.; Abdo Qasem, A. A. Thermal Degradation and Water Uptake of Biodegradable Resin Prepared from Millet Flour and Wheat Gluten Crosslinked with Epoxydized Vegetable Oils. *J. Chem.* **2019** DOI: 10.1155/2019/7050514.
(34) Narute, P.; Rao, G. R.; Misra, S.; Palanisamy, A. Modification of Cottonseed Oil for Amine Cured Epoxy Resin: Studies on Thermo-Mechanical, Physico-Chemical, Morphological and Antimicrobial Properties. *Prog. Org. Coatings* **2015**, *88*, 316−324.
(35) Gaikwad, M. S.; Gite, V. V.; Mahulikar, P. P.; Hundiwale, D. G.; Yemul, O. S. Eco-Friendly Polyurethane Coatings from Cottonseed and Karanja Oil. *Prog. Org. Coatings* **2015**, *86*, 164−172.
(36) Gaddam, S. K.; Kutcherlapati, S. N. R.; Palanisamy, A. Self-Cross-Linkable Anionic Waterborne Polyurethane-Silanol Dispersions from Cottonseed-Oil-Based Phosphorylated Polyol as Ionic Soft Segment. *ACS Sustain. Chem. Eng.* **2017**, *5* (8), 6447−6455.
(37) Chen, Y.; Yasin, A.; Zhang, Y.; Zan, X.; Liu, Y.; Zhang, L. Preparation and Modification of Biomass-Based Functional Rubbers for Removing Mercury(II) from Aqueous Solution. *Mater.* **2020**, *13* (3), 632.
(38) Carbonell-Verdu, A.; Bernardi, L.; Garcia-Garcia, D.; Sanchez-Nacher, L.; Balart, R. Development of Environmentally Friendly Composite Matrices from Epoxidized Cottonseed Oil. *Eur. Polym. J.* **2015**, *63*, 1−10.
(39) Boey, J. Y.; Lee, C. K.; Tay, G. S. Factors Affecting Mechanical Properties of Reinforced Bioplastics: A Review. *Polym.* **2022**, *14* (18), 3737.
(40) Mahmud, S.; Long, Y.; Abu Taher, M.; Xiong, Z.; Zhang, R.; Zhu, J. Toughening Polylactide by Direct Blending of Cellulose Nanocrystals and Epoxidized Soybean Oil. *J. Appl. Polym. Sci.* **2019**, *136* (46), 1−13.
(41) Wu, M.; Zhang, Y.; Peng, Q.; Song, L.; Hu, Z.; Li, Z.; Wang, Z. Mechanically Strong Plant Oil-Derived Thermoplastic Polymers Prepared via Cellulose Graft Strategy. *Appl. Surf. Sci.* **2018**, *458* (June), 495−502.
(42) Clarkson, C. M.; El Awad Azrak, S. M.; Forti, E. S.; Schueneman, G. T.; Moon, R. J.; Youngblood, J. P. Recent Developments in Cellulose Nanomaterial Composites. *Adv. Mater.* **2021**, *33* (28), 14−17.
(43) Retegi, A.; Algar, I.; Martin, L.; Altuna, F.; Stefani, P.; Zuluaga, R.; Gañán, P.; Mondragon, I. Sustainable Optically Transparent Composites Based on Epoxidized Soy-Bean Oil (ESO) Matrix and High Contents of Bacterial Cellulose (BC). *Cellulose* **2012**, *19* (1), 103−109.
(44) Mucci, V. L.; Ivdre, A.; Buffa, J. M.; Cabulis, U.; Stefani, P. M.; Aranguren, M. I. Composites Made from a Soybean Oil Biopolyurethane and Cellulose Nanocrystals. *Polym. Eng. Sci.* **2018**, *58* (2), 125−132.
(45) Song, L.; Wang, Z.; Lamm, M. E.; Yuan, L.; Tang, C. Supramolecular Polymer Nanocomposites Derived from Plant Oils and Cellulose Nanocrystals. *Macromolecules* **2017**, *50* (19), 7475−7483.
(46) Barkane, A.; Kampe, E.; Platnieks, O.; Gaidukovs, S. Cellulose Nanocrystals vs. Cellulose Nanofibers: A Comparative Study of Reinforcing Effects in UV-Cured Vegetable Oil Nanocomposites. *Nanomaterials* **2021**, *11* (7), 1791.
(47) Wang, B.; Zhou, J.; Wang, Z.; Mu, S.; Wu, R.; Wang, Z. Cellulose Nanocrystal/Plant Oil Polymer Composites with Hydrophobicity, Humidity-Sensitivity, and High Wet Strength. *Carbohydr. Polym.* **2020**, *231*, No. 115739.
(48) Zhang, P.; Lu, Y.; Fan, M.; Jiang, P.; Dong, Y. Modified Cellulose Nanocrystals Enhancement to Mechanical Properties and Water Resistance of Vegetable Oil-based Waterborne Polyurethane. *J. Appl. Polym. Sci.* **2019**, *136* (47), No. 48228.
(49) Gao, Z.; Peng, J.; Zhong, T.; Sun, J.; Wang, X.; Yue, C. Biocompatible Elastomer of Waterborne Polyurethane Based on Castor Oil and Polyethylene Glycol with Cellulose Nanocrystals. *Carbohydr. Polym.* **2012**, *87* (3), 2068−2075.
(50) Cordero, A. I.; Amalvy, J. I.; Fortunati, E.; Kenny, J. M.; Chiacchiarelli, L. M. The Role of Nanocrystalline Cellulose on the Microstructure of Foamed Castor-Oil Polyurethane Nanocomposites. *Carbohydr. Polym.* **2015**, *134*, 110−118.
(51) Sain, S.; Åkesson, D.; Skrifvars, M.; Roy, S. Hydrophobic Shape-Memory Biocomposites from Tung-Oil-Based Bioresin and Onion-Skin-Derived Nanocellulose Networks. *Polymers (Basel)* **2020**, *12* (11), 2470.
(52) Börjesson, M.; Westman, G. Crystalline Nanocellulose — Preparation, Modification, and Properties. In *Cellulose—Fundamental Aspects and Current Trends*; InTech, 2015 DOI: 10.5772/61899.
(53) Wang, Y.; Xie, R.; Zheng, S.; Zhou, N.; Lu, J.; Ahmad, I.; Gan, L.; Huang, J. Nonuniformly Modifying High-Aspect-Ratio Rigid

Cellulose Nanocrystals to Enhance Percolation Advantage in Weakly Compatible Biomass Polymer Systems. *Cellulose* **2021**, *28*, 4655−4669.
(54) Jiang, M.-p.; Zhang, J.-h.; Wang, Y.-h.; Ahmad, I.; Guo, X.; Cao, L.-m.; Chen, Y.-k.; Gan, L.; Huang, J. Covalent-Bond-Forming Method to Reinforce Rubber with Cellulose Nanocrystal Based on the Thiol-Ene Click Reaction. *Compos. Commun.* **2021**, *27* (April), No. 100865.
(55) Salmieri, S.; Islam, F.; Khan, R. A.; Hossain, F. M.; Ibrahim, H. M. M.; Miao, C.; Hamad, W. Y.; Lacroix, M. Antimicrobial Nanocomposite Films Made of Poly(Lactic Acid)−Cellulose Nanocrystals (PLA−CNC) in Food Applications—Part B: Effect of Oregano Essential Oil Release on the Inactivation of Listeria Monocytogenes in Mixed Vegetables. *Cellulose* **2014**, *21* (6), 4271−4285.
(56) Yoo, Y.; Youngblood, J. P. Green One-Pot Synthesis of Surface Hydrophobized Cellulose Nanocrystals in Aqueous Medium. *ACS Sustain. Chem. Eng.* **2016**, *4* (7), 3927−3938.
(57) Chakrabarty, A.; Teramoto, Y. Recent Advances in Nanocellulose Composites with Polymers: A Guide for Choosing Partners and How to Incorporate Them. *Polym.* **2018**, *10* (5), 517 DOI: 10.3390/polym10050517.
(58) Zhou, L.; He, H.; Li, M.-c.; Huang, S.; Mei, C.; Wu, Q. Enhancing Mechanical Properties of Poly(Lactic Acid) through Its in-Situ Crosslinking with Maleic Anhydride-Modified Cellulose Nanocrystals from Cottonseed Hulls. *Ind. Crops Prod.* **2018**, *112*, 449−459.
(59) Cao, L.; Huang, J.; Chen, Y. Dual Cross-Linked Epoxidized Natural Rubber Reinforced by Tunicate Cellulose Nanocrystals with Improved Strength and Extensibility. *ACS Sustain. Chem. Eng.* **2018**, *6* (11), 14802−14811.
(60) Ferreira, F. V.; Dufresne, A.; Pinheiro, I. F.; Souza, D. H. S.; Gouveia, R. F.; Mei, L. H. I.; Lona, L. M. F. How Do Cellulose Nanocrystals Affect the Overall Properties of Biodegradable Polymer Nanocomposites: A Comprehensive Review. *Eur. Polym. J.* **2018**, *108*, 274−285.
(61) Pinheiro, I. F.; Ferreira, F. V.; Souza, D. H. S.; Gouveia, R. F.; Lona, L. M. F.; Morales, A. R.; Mei, L. H. I. Mechanical, Rheological and Degradation Properties of PBAT Nanocomposites Reinforced by Functionalized Cellulose Nanocrystals. *Eur. Polym. J.* **2017**, *97*, 356−365.
(62) Garcia-Garcia, D.; Lopez-Martinez, J.; Balart, R.; Strömberg, E.; Moriana, R. Reinforcing Capability of Cellulose Nanocrystals Obtained from Pine Cones in a Biodegradable Poly(3-Hydroxybutyrate)/Poly(ε-Caprolactone) (PHB/PCL) Thermoplastic Blend. *Eur. Polym. J.* **2018**, *104*, 10−18.
(63) Demchuk, Z.; Kingsley, K.; Voronov, A.; Kirianchuk, V.; Shevchuk, O.; Kohut, A.; Voronov, S. Versatile Monomer Platform for Plant Oil-Based Latex Coatings. *Proc. World Congr. New Technol.* **2018**, *1* (6), 11159.
(64) Auclair, N.; Kaboorani, A.; Riedl, B.; Landry, V.; Hosseinaei, O.; Wang, S. Influence of Modified Cellulose Nanocrystals (CNC) on Performance of Bionanocomposite Coatings. *Prog. Org. Coatings* **2018**, *123* (May), 27−34.
(65) Wang, B.; Zhou, J.; Wang, Z.; Mu, S.; Wu, R.; Wang, Z. Cellulose Nanocrystal/Plant Oil Polymer Composites with Hydrophobicity, Humidity-Sensitivity, and High Wet Strength. *Carbohydr. Polym.* **2020**, *231*, No. 115739.
(66) Wijayapala, R.; Mishra, S.; Elmore, B.; Freeman, C.; Kundu, S. Synthesis and Characterization of Crosslinked Polymers from Cottonseed Oil. *J. Appl. Polym. Sci.* **2019**, *136* (24), No. 47655.
(67) Foster, E. J.; Moon, R. J.; Agarwal, U. P.; Bortner, M. J.; Bras, J.; Camarero-Espinosa, S.; Chan, K. J.; Clift, M. J. D.; Cranston, E. D.; Eichhorn, S. J.; Fox, D. M.; Hamad, W. Y.; Heux, L.; Jean, B.; Korey, M.; Nieh, W.; Ong, K. J.; Reid, M. S.; Renneckar, S.; Roberts, R.; Shatkin, J. A.; Simonsen, J.; Stinson-Bagby, K.; Wanasekara, N.; Youngblood, J. Current Characterization Methods for Cellulose Nanomaterials. *Chem. Soc. Rev.* **2018**, *47* (8), 2609−2679.
(68) Kim, Y.; McCoy, L. T.; Lee, E.; Lee, H.; Saremi, R.; Feit, C.; Hardin, I. R.; Sharma, S.; Mani, S.; Minko, S. Environmentally Sound Textile Dyeing Technology with Nanofibrillated Cellulose. *Green Chem.* **2017**, *19* (17), 4031−4035.
(69) Annisa, A. N.; Widayat, W. A Review of Bio-Lubricant Production from Vegetable Oils Using Esterification Transesterification Process. *MATEC Web Conf.* **2018**, *156*, 06007.
(70) Dinda, S.; Patwardhan, A. V.; Goud, V. V.; Pradhan, N. C. Epoxidation of Cottonseed Oil by Aqueous Hydrogen Peroxide Catalysed by Liquid Inorganic Acids. *Bioresour. Technol.* **2008**, *99* (9), 3737−3744.
(71) Maleic anhydride SDS, Safety Data Sheets - ECHEMI https://www.echemi.com/sds/maleic-anhydride-pd1805231002.html (accessed Oct 27, 2022).
(72) Zhou, L.; Ke, K.; Yang, M. B.; Yang, W. Recent Progress on Chemical Modification of Cellulose for High Mechanical-Performance Poly(Lactic Acid)/Cellulose Composite: A Review. *Compos. Commun.* **2021**, *23*, No. 100548.
(73) Khan, M.; Shah, L. A.; Rahman, T. U.; Yoo, H. M.; Ye, D.; Vacharasin, J. Cellulose Nanocrystals Boosted Hydrophobic Association in Dual Network Polymer Hydrogels as Advanced Flexible Strain Sensor for Human Motion Detection. *J. Mech. Behav. Biomed. Mater.* **2023**, *138*, No. 105610.
(74) Seo, Y.-R.; Kim, J.-W.; Hoon, S.; Kim, J.; Chung, J. H.; Lim, K.-T. Cellulose-Based Nanocrystals: Sources and Applications via Agricultural Byproducts. *J. Biosyst. Eng.* **2018**, *43* (1), 59−71.
(75) Yu, H. Y.; Qin, Z. Y.; Yan, C. F.; Yao, J. M. Green Nanocomposites Based on Functionalized Cellulose Nanocrystals: A Study on the Relationship between Interfacial Interaction and Property Enhancement. *ACS Sustain. Chem. Eng.* **2014**, *2* (4), 875−886.
(76) Yu, H. Y.; Yao, J. M. Reinforcing Properties of Bacterial Polyester with Different Cellulose Nanocrystals via Modulating Hydrogen Bonds. *Compos. Sci. Technol.* **2016**, *136*, 53−60.
(77) Miao, C.; Mauran, D.; Hamad, W. Y. How Hydrogen-Bonding Interactions and Nanocrystal Aspect Ratios Influence the Morphology and Mechanical Performance of Polymer Nanocomposites Reinforced with Cellulose Nanocrystals. *Soft Matter* **2022**, *18* (24), 4572−4581.
(78) Saithai, P.; Lecomte, J.; Dubreucq, E.; Tanrattanakul, V. Effects of Different Epoxidation Methods of Soybean Oil on the Characteristics of Acrylated Epoxidized Soybean Oil-Co-Poly(Methyl Methacrylate) Copolymer. *Express Polym. Lett.* **2013**, *7* (11), 910−924.
(79) Pradhan, S.; Pandey, P.; Mohanty, S.; Nayak, S. K. Synthesis and Characterization of Waterborne Epoxy Derived from Epoxidized Soybean Oil and Bioderived C-36 Dicarboxylic Acid. *J. Coatings Technol. Res.* **2017**, *14* (4), 915−926.
(80) Wang, C.-S.; Yang, L.-T.; Ni, B.-L.; Shi, G. Polyurethane Networks from Different Soy-Based Polyols by the Ring Opening of Epoxidized Soybean Oil with Methanol, Glycol, and 1,2-Propanediol. *J. Appl. Ploym. Sci.* **2009**, *114* (1), 125−131.
(81) Pour-Esmaeil, S.; Sharifi-Sanjani, N.; Khoee, S.; Taheri-Qazvini, N. Biocompatible Chemical Network of α-Cellulose-ESBO (Epoxidized Soybean Oil) Scaffold for Tissue Engineering Application. *Carbohydr. Polym.* **2020**, *241* (March), No. 116322.
(82) Sahoo, S. K.; Mohanty, S.; Nayak, S. K. Toughened Bio-Based Epoxy Blend Network Modified with Transesterified Epoxidized Soybean Oil: Synthesis and Characterization. *RSC Adv.* **2015**, *5* (18), 13674−13691.
(83) Mohamed, A. A.; Hussain, S.; Alamri, M. S.; Ibraheem, M. A.; Qasem, A. A. A. Amidolysis of Oxirane: Effect of Protein Type, Oils, and $ZnCl_2$ on the Rheological Properties of Cross-Linked Protein and Oxirane. *Int. J. Polym. Sci.* **2018**, *2018*, 1.
(84) Nicolau, A.; Mariath, R. M.; Martini, E. A.; dos Santos Martini, D.; Samios, D. The Polymerization Products of Epoxidized Oleic Acid and Epoxidized Methyl Oleate with Cis-1,2-Cyclohexanedicarboxylic Anhydride and Triethylamine as the Initiator: Chemical Structures, Thermal and Electrical Properties. *Mater. Sci. Eng. C* **2010**, *30* (7), 951−962.
(85) Li, M.; Xia, J.; Mao, W.; Yang, X.; Xu, L.; Huang, K.; Li, S. Preparation and Properties of Castor Oil-Based Dual Cross-Linked

Polymer Networks with Polyurethane and Polyoxazolidinone Structures. *ACS Sustain. Chem. Eng.* **2017**, *5* (8), 6883−6893.
(86) Farooq, U.; Teuwen, J.; Dransfeld, C. Toughening of Epoxy Systems with Interpenetrating Polymer Network (IPN): A Review. *Polym.* **2020**, *12* (9), 1908.
(87) Kashani Rahimi, S.; Aeinehvand, R.; Kim, K.; Otaigbe, J. U. Structure and Biocompatibility of Bioabsorbable Nanocomposites of Aliphatic-Aromatic Copolyester and Cellulose Nanocrystals. *Biomacromolecules* **2017**, *18* (7), 2179−2194.
(88) Teixeira, L. T.; Braz, W. F.; Correia de Siqueira, R. N.; Pandoli, O. G.; Geraldes, M. C. Sulfated and Carboxylated Nanocellulose for Co+2 Adsorption. *J. Mater. Res. Technol.* **2021**, *15*, 434−447.
(89) Germiniani, L. G. L.; da Silva, L. C. E.; Plivelic, T. S.; Gonçalves, M. C. Poly(ε-Caprolactone)/Cellulose Nanocrystal Nanocomposite Mechanical Reinforcement and Morphology: The Role of Nanocrystal Pre-Dispersion. *J. Mater. Sci.* **2019**, *54* (1), 414−426.
(90) Jardin, J. M.; Zhang, Z.; Hu, G.; Tam, K. C.; Mekonnen, T. H. Reinforcement of Rubber Nanocomposite Thin Sheets by Percolation of Pristine Cellulose Nanocrystals. *Int. J. Biol. Macromol.* **2020**, *152*, 428−436.
(91) Sonseca, Á.; Camarero-Espinosa, S.; Peponi, L.; Weder, C.; Foster, E. J.; Kenny, J. M.; Giménez, E. Mechanical and Shape-Memory Properties of Poly(Mannitol Sebacate)/Cellulose Nanocrystal Nanocomposites. *J. Polym. Sci. Part A Polym. Chem.* **2014**, *52* (21), 3123−3133.
(92) Leite, L. S. F.; Battirola, L. C.; da Silva, L. C. E.; Gonçalves, M. do C. Morphological Investigation of Cellulose Acetate/Cellulose Nanocrystal Composites Obtained by Melt Extrusion. *J. Appl. Polym. Sci.* **2016**, *133* (44), 1−10.
(93) Miao, C.; Hamad, W. Y. Critical Insights into the Reinforcement Potential of Cellulose Nanocrystals in Polymer Nanocomposites. *Curr. Opin. Solid State Mater. Sci.* **2019**, *23* (4), No. 100761.
(94) Azizi Samir, M. A. S.; Alloin, F.; Dufresne, A. Review of Recent Research into Cellulosic Whiskers, Their Properties and Their Application in Nanocomposite Field. *Biomacromolecules* **2005**, *6* (2), 612−626.
(95) Mariano, M.; El Kissi, N.; Dufresne, A. Cellulose Nanocrystals and Related Nanocomposites: Review of Some Properties and Challenges. *J. Polym. Sci., Part B: Polym. Phys.* **2014**, *52* (12), 791−806.
(96) Sonseca, Á.; Camarero-Espinosa, S.; Peponi, L.; Weder, C.; Foster, E. J.; Kenny, J. M.; Giménez, E. Mechanical and Shape-Memory Properties of Poly(Mannitol Sebacate)/Cellulose Nanocrystal Nanocomposites. *J. Polym. Sci. Part A Polym. Chem.* **2014**, *52* (21), 3123−3133.
(97) Moon, R. J.; Martini, A.; Nairn, J.; Simonsen, J.; Youngblood, J. *Cellulose Nanomaterials Review: Structure, Properties and Nanocomposites*; 2011; Vol. *40* DOI: 10.1039/c0cs00108b.
(98) Tien, Y. I.; Wei, K. H. Hydrogen Bonding and Mechanical Properties in Segmented Montmorillonite/Polyurethane Nanocomposites of Different Hard Segment Ratios. *Polymer (Guildf)* **2001**, *42* (7), 3213−3221.
(99) Pei, A.; Malho, J. M.; Ruokolainen, J.; Zhou, Q.; Berglund, L. A. Strong Nanocomposite Reinforcement Effects in Polyurethane Elastomer with Low Volume Fraction of Cellulose Nanocrystals. *Macromolecules* **2011**, *44* (11), 4422−4427.
(100) Shojaeiarani, J.; Bajwa, D. S.; Chanda, S. Cellulose Nanocrystal Based Composites: A Review. *Compos. Part C Open Access* **2021**, *5*, No. 100164.
(101) Ustunel, S.; Prévôt, M. E.; Rohaley, G. A. R.; Webb, C. R.; Yavitt, B.; Freychet, G.; Zhernenkov, M.; Pindak, R.; Schaible, E.; Zhu, C.; Hegmann, T.; Clements, R. J.; Hegmann, E. Mechanically Tunable Elastomer and Cellulose Nanocrystal Composites as Scaffolds for in Vitro Cell Studies. *Mater. Adv.* **2021**, *2* (1), 464−476.
(102) Gao, M.; Wang, Y.; Li, S.; Liu, J.; Feng, A.; Zhang, G.; Zhang, L. Design and Fabrication of Recyclable and Reshape Vitrified Elastomer Reinforced with Renewable Cellulose Nanocrystal. *Compos. Commun.* **2022**, *32*, No. 101165.
(103) Sultana, T.; Sultana, S.; Nur, H. P.; Khan, M. W. Studies on Mechanical, Thermal and Morphological Properties of Betel Nut Husk Nano Cellulose Reinforced Biodegradable Polymer Composites. *J. Compos. Sci.* **2020**, *4* (3), 83.
(104) Khelifa, F.; Habibi, Y.; Bonnaud, L.; Dubois, P. Epoxy Monomers Cured by High Cellulosic Nanocrystal Loading. *ACS Appl. Mater. Interfaces* **2016**, *8* (16), 10535−10544.
(105) Aguayo, M.; Fernandez Perez, A.; Reyes, G.; Oviedo, C.; Gacitua, W.; Gonzalez, R.; Uyarte, O. Isolation and Characterization of Cellulose Nanocrystals from Rejected Fibers Originated in the Kraft Pulping Process. *Polym.* **2018**, *10* (10), 1145.
(106) Larissa, L. A.; Fonsêca, A. F.; Pereira, F. V.; Druzian, J. I. Extraction and Characterization of Cellulose Nanocrystals from Corn Stover. *Cellul. Chem. Technol.* **2015**, *49* (2), 127−133.
(107) Shang, Q.; Liu, C.; Hu, Y.; Jia, P.; Hu, L.; Zhou, Y. Bio-Inspired Hydrophobic Modification of Cellulose Nanocrystals with Castor Oil. *Carbohydr. Polym.* **2018**, *191*, 168−175.
(108) Buffa, J. M.; Mondragon, G.; Corcuera, M. A.; Eceiza, A.; Mucci, V.; Aranguren, M. I. Physical and Mechanical Properties of a Vegetable Oil Based Nanocomposite. *Eur. Polym. J.* **2018**, *98*, 116−124.
(109) Mi, H. Y.; Jing, X.; Peng, J.; Salick, M. R.; Peng, X. F.; Turng, L. S. Poly(ε-Caprolactone) (PCL)/Cellulose Nano-Crystal (CNC) Nanocomposites and Foams. *Cellulose* **2014**, *21* (4), 2727−2741.
(110) Lu, P.; Hsieh, Y. Lo. Cellulose Isolation and Core-Shell Nanostructures of Cellulose Nanocrystals from Chardonnay Grape Skins. *Carbohydr. Polym.* **2012**, *87* (4), 2546−2553.
(111) Rasheed, M.; Jawaid, M.; Parveez, B.; Zuriyati, A.; Khan, A. Morphological, Chemical and Thermal Analysis of Cellulose Nanocrystals Extracted from Bamboo Fibre. *Int. J. Biol. Macromol.* **2020**, *160*, 183−191.